Structural basis for antiactivation in bacterial quorum sensing

Guozhou Chen*, Philip D. Jeffrey†, Clay Fuqua*, Yigong Shi†, and Lingling Chen*‡

*Department of Biology, Indiana University, 915 East Third Street, Bloomington, IN 47405; and †Department of Molecular Biology, Princeton University, Princeton, NJ 08544

Bacteria can communicate via diffusible signal molecules they generate and release to coordinate their behavior in response to the environment. Signal molecule concentration is often proportional to bacterial population density, and when this reaches a critical concentration, reflecting a bacterial quorum, specific behaviors including virulence, symbiosis, and horizontal gene transfer are activated. Quorum-sensing regulation in many Gram-negative bacteria involves acylated homoserine lactone signals that are perceived through binding to LuxR-type, acylated-homoserine-lactone-responsive transcription factors. Bacteria of the rhizobial group employ the LuxR-type transcriptional activator TraR in quorum sensing, and its activity is further regulated through interactions with the TraM antiactivator. In this study, we have crystallographically determined the 3D structure of the TraR–TraM antiactivation complex from *Rhizobium* sp. strain NGR234. Unexpectedly, the antiactivator TraM binds to TraR at a site distinct from its DNA-binding motif and induces an allosteric conformational change in the protein, thereby preventing DNA binding. Structural analysis reveals a highly conserved TraR–TraM interface and suggests a mechanism for antiactivation complex formation. This structure may inform alternative strategies to control quorum-sensing-regulated microbial activity including amelioration of infectious disease and antibiotic resistance. In addition, the structural basis of antiactivation presents a regulatory interaction that provides general insights relevant to the field of transcription regulation and signal transduction.

crystal structure | TraR–TraM complex | allosteric mechanism | protein–protein interaction | signal transduction

Bacteria can release signal molecules into their environment and subsequently respond to these same signals, as a measure of their own population density (1). Generally known as quorum sensing, this mechanism regulates processes such as virulence, symbiosis, and horizontal gene transfer, which are of adaptive benefit in dense populations and are typified by processes associated with host organisms. Bacteria within the large and diverse proteobacterial group use acylated homoserine lactones (AHLs) as quorum-sensing signal molecules (2). AHLs are usually synthesized via enzymes of the LuxI family, and the response to these signals is typically mediated through transcription factors of the LuxR family. There has been intense interest in studying the molecular mechanisms of quorum sensing to develop strategies by which to control microbial activity. Inhibition of AHL quorum sensing through chemically synthesized AHL analogs, inhibitory natural products, and AHL-degrading enzymes has achieved variable degrees of effectiveness (3). Inhibition mechanisms, however, are still required and offer the promise of ameliorating infectious disease through modulation of intercellular communication.

Proteobacteria within the *Rhizobiaceae* and *Bradyrhizobiaceae* families express homologs of the TraM protein, a potent antiactivator protein originally identified in *Agrobacterium tumefaciens* that blocks the activity of its associated LuxR-type transcription factor, TraR. TraM inhibits TraR in several different microbial taxa and is often required to maintain the quorum-sensing mechanism in the

inactive state (4–7). TraM inhibits quorum sensing by direct binding to TraR, preventing it from binding to its DNA target promoters (8, 9). Although the structure of TraM from *A. tumefaciens* has been solved recently (10–12), this discovery has provided only limited insight into the mechanism of TraR inhibition. We now report the 3D structure of the TraM (TraM$_{NGR}$) inhibitor from *Rhizobium* species strain NGR234 in complex with its cognate TraR transcription factor (TraR$_{NGR}$). The novel configuration of this complex distinguishes several competing models for the inhibitory activity of TraM and suggests that heterocomplex formation allosterically and indirectly modifies the conformation of the TraR DNA binding domain, thereby blocking association with target promoters.

Results

Biochemical Characterizations. In solution, TraM$_{NGR}$ (theoretical molecular mass of 14.37 kDa) existed as a molecular species of 17.6 and 14.5 kDa by gel filtration and analytical ultracentrifugation (AUC) experiments [supporting information (SI) Fig. 5*A*], respectively, consistent with monomeric TraM$_{NGR}$. Purified TraR$_{NGR}$ (monomer molecular mass of 26.29 kDa) eluted by gel filtration at 44.5 kDa and sedimented in AUC at 53.4 kDa (SI Fig. 5*B*); both values were consistent with a homodimeric structure. Isothermal titration calorimetry (ITC) suggested that TraM binds to TraR in a 1:1 molar ratio, with a disassociation constant (K_d) of 14.9 nM (Fig. 1*A*). The molecular mass of the TraR–TraM complex (theoretical molecular mass of 81.32 kDa), as derived from AUC, was 83.2 kDa (Fig. 1*B*), which was indicative of a heterotetramer (TraR$_{NGR}$–TraM$_{NGR}$)$_2$.

Overall Structure of TraR$_{NGR}$–TraM$_{NGR}$. TraR$_{NGR}$–TraM$_{NGR}$ crystallized in the P$_1$ space group with one heterotetramer complex per asymmetric unit. TraR$_{NGR}$ was organized into two structural and functional domains: the N-terminal dimerization domain (NTD) (1–164 aa) and the C-terminal DNA-binding domain (CTD) (175–236 aa). In the structure, the two NTDs of the complex were related by a rotational C2 symmetry. Interestingly, CTDs were located asymmetrically relative to their respective NTDs. In one monomer (Fig. 2*A*), the CTD was packed over its NTD via an 11-aa linker that looped back (the closed form). In the second monomer, the CTD swung far from its NTD (the open form) and the linker adopted an extended conformation. In the closed
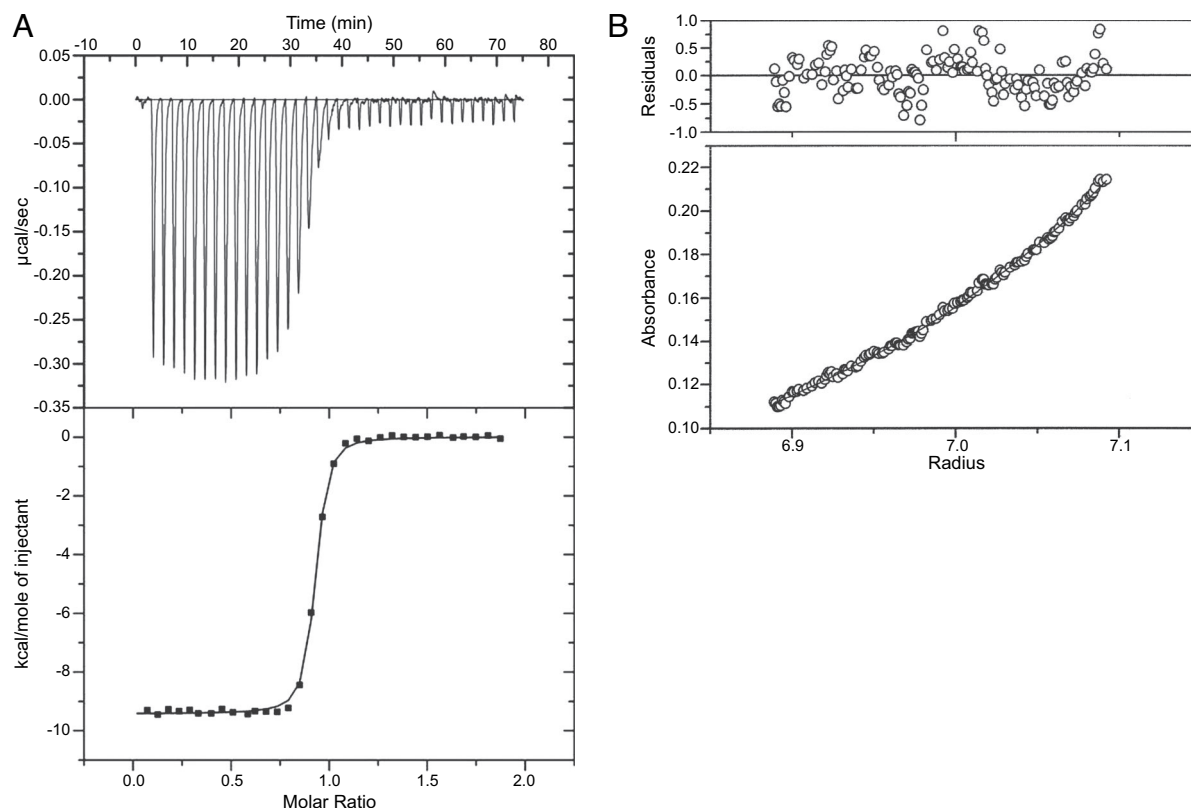

Fig. 1. Biochemical characterizations of the TraR$_{NGR}$–TraM$_{NGR}$ complex. (*A*) ITC analysis of the TraR$_{NGR}$–TraM$_{NGR}$ interaction. A single binding site was used to fit the data and to derive thermodynamic parameters. (*B*) AUC sedimentation equilibrium studies on the TraR$_{NGR}$–TraM$_{NGR}$ complex. A single species model was used to fit data. Data fitting (*Upper*) and the fitting residual (*Lower*) are shown.

form, TraM$_{NGR}$ was sandwiched between the TraR$_{NGR}$ NTD and CTD, interacting with both domains. The interaction with the NTD was, however, completely disrupted in the open form, and the resulting extended conformation was stabilized by contact with the neighboring TraR$_{NGR}$–TraM$_{NGR}$ in the crystal. Without crystal packing, it is possible that both TraR$_{NGR}$ protomers would adopt the closed conformation, each TraM$_{NGR}$ interacting with the NTD and CTD of a single TraR$_{NGR}$ pro-

tomer. A model of (TraR$_{NGR}$–TraM$_{NGR}$)$_2$ was thus generated assuming that the two TraR$_{NGR}$–TraM$_{NGR}$ pairs follow the C2 rotational symmetry identified in NTDs, and no steric clashes were observed (Fig. 2*B*).

Interaction Between TraR$_{NGR}$ and TraM$_{NGR}$. The interactions between the CTD and TraM$_{NGR}$ were maintained in both the open and closed conformations of TraR$_{NGR}$. The TraR$_{NGR}$ CTD
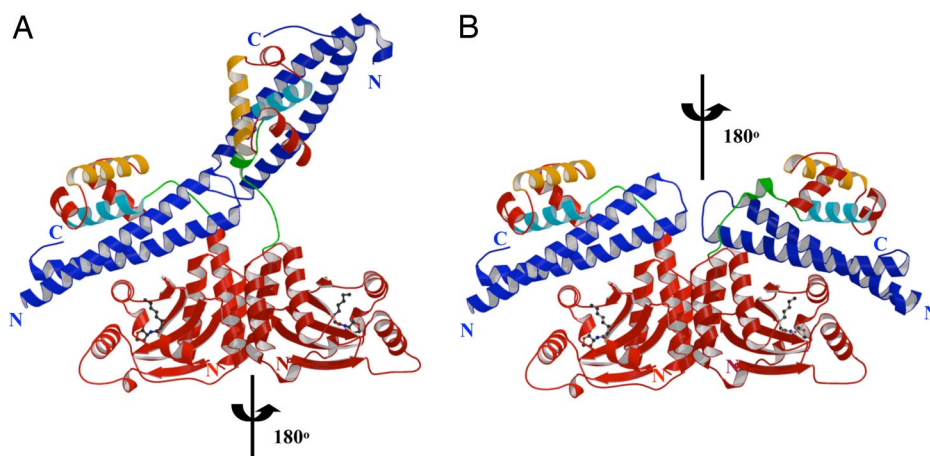

Fig. 2. Overall structure of the TraR$_{NGR}$–TraM$_{NGR}$ complex. (*A*) Structure of tetrameric NGR234 TraR–TraM complex. The TraR$_{NGR}$–TraM$_{NGR}$ pair in the closed conformation is colored red and blue, respectively, whereas the other pair in the open conformation is in dark red and dark blue, respectively. The ligand AHL is shown in a ball-and-stick representation. α10, the major TraM-binding site, and α12, the DNA recognition helix, are colored in cyan and orange, respectively. The linker is colored in green. (*B*) Model of symmetric (TraR$_{NGR}$–TraM$_{NGR}$)$_2$ in solution. The model was generated by applying the C2 rotational symmetry of the NTDs to the closed conformation of dimeric TraR$_{NGR}$–TraM$_{NGR}$. No structural conflicts are observed in the symmetric model. Views of *A* and *B* are the same. The figures were generated by using MOLSCRIPT and RASTER 3D (28, 29).

residues in α10 and α11 provided the majority of contacts with TraM$_{NGR}$. L182, W186, and P178 of α10 projected their side chains into the groove formed between the two long helices of TraM$_{NGR}$. Mutational analysis of the *A. tumefaciens* system (TraR$_{At}$–TraM$_{At}$) has revealed that modification of P178 and L182 either decreases or abolishes the antiactivation of TraR$_{At}$ by TraM$_{At}$ (9). In the TraR$_{NGR}$–TraM$_{NGR}$ structure, W186, conserved among LuxR-type proteins (SI Fig. 6), was completely buried by a pocket formed by H39, Q85, L88, and L92 of TraM$_{NGR}$ (Fig. 3*A*). Besides nonspecific van der Waals interactions, atom NE1 of W186 formed intermolecular hydrogen bonds with both NE2 of H39 and OE1 of Q85 (Fig. 3*A*). For α11, the interaction is primarily via a hydrophobic cluster with the C-terminal end of TraM$_{NGR}$, a region that has been implicated in TraR binding for TraM$_{At}$ (8). L199 was located at the center of this cluster (Fig. 3*B*) and was also conserved (L or I) among LuxR proteins (SI Fig. 6).

Similarly, the TraM residues that participate in the TraR–TraM interaction were also conserved. TraM$_{NGR}$ H39 and Q85 interacted with TraR$_{NGR}$ W186 and were conserved among most TraM proteins (Fig. 3*D*). Several other conserved TraM$_{NGR}$ residues were engaged in hydrogen bond interactions with TraR$_{NGR}$: (*i*) Y74 was centered within an extensive nine-residue intermolecular hydrogen-bonding network (Fig. 3*C*); (*ii*) R40 was hydrogen bonded to L199 and N198; and (*iii*) Q71 hydrogen bonded with L170. All of the hydrogen bonds involving these three conserved TraM residues (R40, Q71, and Y74) occurred between TraM$_{NGR}$ side chains and backbone atoms of TraR$_{NGR}$, and therefore these interactions were somewhat independent of the TraR primary sequence. Although the W186 (TraR) side chain contributed to hydrogen bonding (described above), the conserved nature of this residue suggests that these hydrogen bonds are general to TraM–TraR interactions and that W186 plays a critical role in recognizing specific TraM side chains during complex formation. Taken together, these findings suggest that the extensive and complex intermolecular hydrogen bond patterns observed in NGR234 should be general to the TraR–TraM interaction in related systems. These findings provide structural information that largely corroborates the extensive mutational analyses of TraR and TraM proteins from *A. tumefaciens* (8, 13, 14). Some of the corresponding residues are clearly implicated in the NGR234 antiactivation complex structure, whereas others may play transient roles in complex formation or additional ancillary functions.

In the closed conformation of TraR$_{NGR}$, the NTD also interacted with TraM$_{NGR}$ but less extensively. Notably, none of the interacting residues was conserved within either the TraM or TraR families. A much smaller surface area was sequestered within TraR$_{NGR}$NTD–TraM$_{NGR}$ contacts ($≈988$ Å²) than by those of TraR$_{NGR}$CTD–TraM$_{NGR}$ ($≈2,180$ Å²). The minor role of the NTD in binding of TraM$_{NGR}$ may account for the open conformation in the crystal, where its interactions with TraM$_{NGR}$ were disrupted. These structural observations were consistent with previous mutational analysis on TraR$_{At}$, which have suggested that the TraR CTD is mainly responsible for TraM interactions (9).

The flexible linker (residues 165–174), which tethered the TraR CTD and NTD, also interacted with TraM$_{NGR}$, and this mode of the interaction was preserved in both the open and closed conformations. In particular, the L170 and P172 backbones of TraR$_{NGR}$ were hydrogen bonded to the conserved TraM$_{NGR}$ residues Q71 and Y50, a less well conserved position in the protein (Fig. 3*D*).

Structures of TraM$_{NGR}$ and TraR$_{NGR}$. TraM$_{NGR}$ folded into two long antiparallel α-helices, similar to the structure of monomeric TraM$_{At}$ from *A. tumefaciens* (10–12). The two-helix bundles of two adjacent TraM$_{At}$ molecules further interacted to promote a homodimeric structure, stabilized by the hydrophobic molecular surface of TraM$_{At}$ that was largely buried along the dimer interface. Mutational studies indicate that this configuration maintains the stability of TraM$_{At}$ (10). Notably, the positions of hydrophobic residues sequestered within the dimer interface of TraM$_{At}$ (L14, L17, L20, I70, and I77) contained charged or polar residues in TraM$_{NGR}$ (N13, K16, R19, E73, and K79). TraM$_{NGR}$ was primarily hydrophilic on the surface and thus was able to exist as a monomer, as indicated by both gel filtration and AUC studies.

TraR$_{NGR}$ was similar to TraR$_{At}$ (44.1% sequence homology; SI Fig. 6), the crystal structure of which, with its AHL and a DNA target sequence (the activation complex), has been solved (15, 16). As with TraR$_{At}$, the TraR$_{NGR}$ NTD contains the AHL-binding site including the essential D72 residue (14), with the AHL molecule embedded within a largely hydrophobic core of this domain. The helical TraR$_{NGR}$ CTD contains the DNA recognition helix (α12), which functions to interact with target DNA sequences through the major groove (7, 15, 16). The overall structure of the TraR NTD and CTD in the TraR$_{NGR}$–TraM$_{NGR}$ antiactivation complex and the TraR$_{At}$–DNA complex overlayed well with rmsds of <2.5 and <1.2 Å, respectively.

The relative orientation of the TraR CTD with respect to its NTD varied greatly between the *A. tumefaciens* and NGR234 complexes and also between protomers within the same complex. In TraR$_{NGR}$–TraM$_{NGR}$, one of the TraR$_{NGR}$ CTDs along with the bound TraM$_{NGR}$ was articulated to make nonspecific contacts with the neighboring molecule because of crystal packing. In the TraR$_{At}$–DNA complex, the two CTDs shift independently to present α12 in an optimal distance and orientation to make contact with the DNA (15, 16). When the entire *A. tumefaciens* and NGR234 complexes were superimposed on the NTD, the CTD orientation varied drastically (Fig. 4*A*). These findings suggest that each CTD can move as a discrete unit, independent from the NTD, that may adopt various orientations owing to the flexible linker between the CTD and NTD. Fig. 4*A* shows that this linker also underwent a remarkable structural shift upon TraM binding. In the TraR$_{At}$–DNA activation complex, the linker is exposed on the surface of the complex (15, 16). In the TraR$_{NGR}$–TraM$_{NGR}$ complex, the linker was found to be rotated 180° around I163 and to be sequestered along the dimeric interface formed by the TraR NTDs. Consequently, the DNA recognition helix (α12) was found to be rotated $≈90°$, well out of position to interact with the DNA major groove.

Discussion

It is clear that TraM can associate with TraR that is free in solution, as well as with TraR that is preassociated at a DNA-binding site (8, 10, 11, 13). For free TraR, our findings with the NGR234 complex suggest a relatively simple mechanism. TraM$_{NGR}$ monomers bind independently to each TraR protomer in the TraR$_{NGR}$ dimer. It may be that binding of the first TraM$_{NGR}$ promotes binding of the second TraM$_{NGR}$ because the tetrameric TraM–TraR NGR234 complex was the dominant species observed *in vitro*. Consistent with this, the conformational changes induced in one protomer of TraR$_{NGR}$ upon TraM binding would likely make α10 in the adjacent protomer more accessible.

A more complex mechanism must be considered for interactions between TraM and TraR that is already bound to DNA. The NGR234 TraR–TraM complex revealed the positions that provide important contacts with TraR. The corresponding positions on TraR, encompassed by the linker and α10, were readily accessible in the TraR$_{At}$–DNA complex (Fig. 4*A*). A mechanism was suggested by which TraM might disengage TraR that is already associated with its DNA-binding site (Fig. 4*B*). We describe this model in terms of the NGR234 tetrameric complex, but similar mechanisms could also lead to the octameric *A. tumefaciens* complex from a preformed TraR–DNA complex.
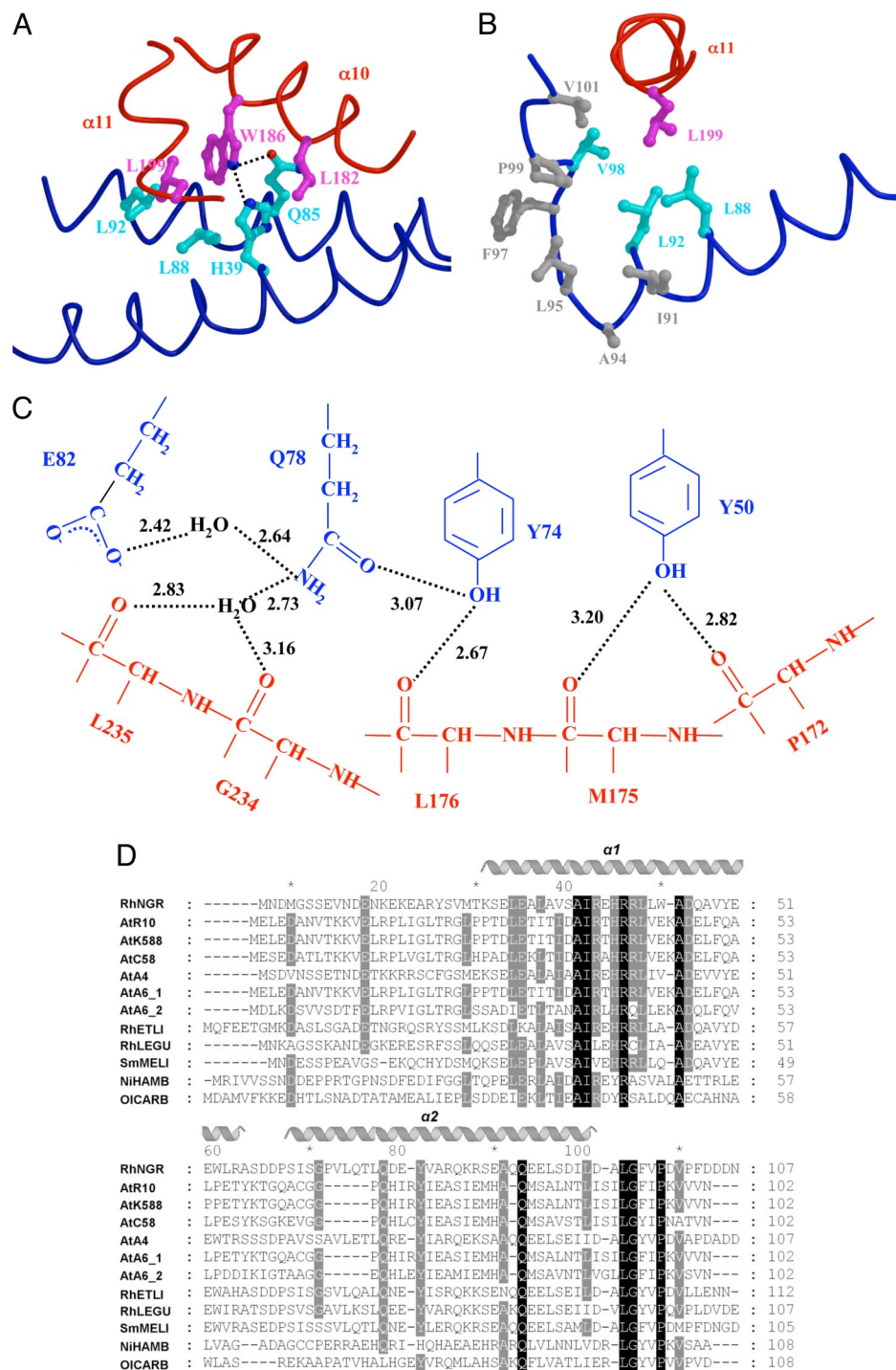
Fig. 3. Structural analysis of the TraR$_{NGR}$–TraM$_{NGR}$ complex. (*A*) The TraR$_{NGR}$–TraM$_{NGR}$ interactions at TraR$_{NGR}$ W186. Side chains from TraR$_{NGR}$ are colored in magenta, and those from TraM$_{NGR}$ are in cyan. The oxygen atom is in red, and nitrogen atoms are in blue. (*B*) Interactions of TraR$_{NGR}$ L199 (in magenta) with the hydrophobic cluster at the C termini of TraM$_{NGR}$. Hydrophobic side chains of the cluster are colored in gray, whereas those that interact directly with L199 are colored in cyan. (*C*) The extensive intermolecular hydrogen-bonding network. Residues from TraM$_{NGR}$ and TraR$_{NGR}$ are colored in blue and red, respectively. The values (in angstroms) denote the distance between hydrogen donors and acceptors. Only interacting moieties, i.e., side chains of TraM$_{NGR}$ and backbones of TraR$_{NGR}$, are shown. (*D*) Multiple sequence alignment of the antiactivator TraM proteins by using CLUSTALW (30). Amino acid sequences are from the following bacteria: RhNGR (or TraM$_{NGR}$ in the text), *Rhizobium* sp. NGR234; AtR10 (TraM$_{At}$), *A. tumefaciens* R10; AtK588, *A. tumefaciens* K588; ATC58, *A. tumefaciens* C58; AtA4, *A. tumefaciens* A4; AtA6_1, *A. tumefaciens* A6; AtA6_2, *A. tumefaciens* A6 *traM2*; RhETLI, *Rhizobium etli* CFN42; RhLEGU, *R. leguminosarum*; SmMELI, *Sinorhizobium meliloti* AK631; and NiHAMB, *Nitrobacter hamburgensis* X14; OlCARB, *Oligotropha carboxidovorans*. Invariant residues are highlighted in black, and highly conserved resides are shaded in grey. Secondary structure elements of TraM$_{NGR}$ are indicated above. *A* and *B* were generated by using MOLSCRIPT and RASTER 3D (28, 29).

Briefly, one TraM may bind to the exposed linker and α10 of one TraR protomer in the TraR$_2$–DNA complex. Binding of TraM drives the linker to rotate inward and repositions α12, thereby disengaging this TraR protomer from its half-site on the DNA. In the TraR$_{At}$–DNA structure, α10 of the other TraR protomer is buried within the structure. Upon the dissociation of the first
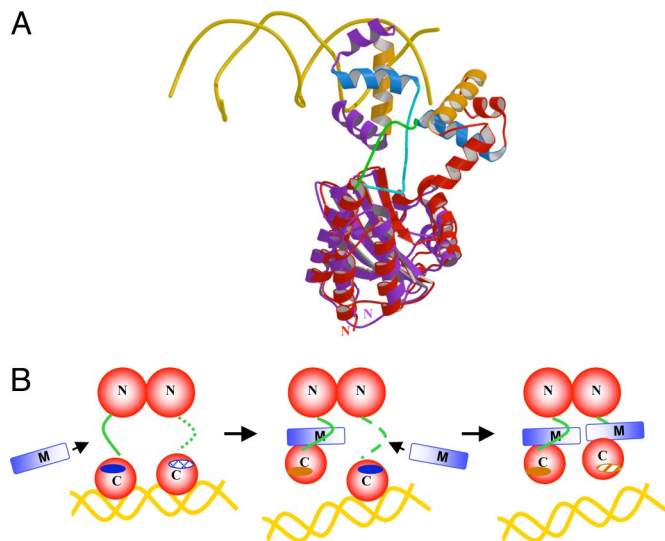
A

B

Fig. 4. Mechanism of TraM inhibition of TraR. (*A*) Comparison of TraR$_{At}$–DNA with TraR$_{NGR}$–TraM$_{NGR}$ structures. The NTDs of the both structures are superimposed, but for clarity, only one protomer of TraR$_{NGR}$ (in red) and TraR$_{At}$ (in purple) from each structure is shown. α10, the TraR helix primarily responsible for TraM interactions, is light blue, and α12, the DNA binding helix, is orange. DNA is displayed as a double coil and is gold. The linker of TraR$_{NGR}$ is highlighted in green, and that of TraR$_{At}$ is in cyan. The image was generated by using MOLSCRIPT and RASTER 3D (28, 29). (*B*) The proposed stepwise dissociation of TraR$_{NGR}$–DNA by TraM$_{NGR}$. One of the linkers in TraR–DNA, disordered and thus not observed crystallographically, is represented by the dotted line. The exposed TraM-binding site is indicated by a dark blue solid oval, and the buried site is denoted by a hatch-filled oval. The DNA-binding site facing the reader is represented as a dark orange solid oval, and that facing away from the reader as a shaded oval.

TraR protomer from the DNA by TraM, the buried α10 would be exposed, allowing it to interact with a second TraM that may already have associated with the TraR linker region. Such a stepwise dissociation, coupled with the strong affinity of TraM to TraR (K_d of 14.9 nM; described above), would promote disruption of cooperativity and hence destabilize the binding of homodimeric TraR to DNA. This mechanism suggests that a transient ternary complex (TraM–TraR$_2$–DNA) may form, although this may be very short lived. This ternary intermediate has been detected in *A. tumefaciens* when incubating TraM$_{At}$ with the TraR$_{At}$–DNA complex (13).

Transcription factors often bind specific sequences associated with target genes. Antiactivators from several systems appear to occupy sites on the transcription factors that would otherwise coordinate specific base contacts on the DNA, thereby precluding or inhibiting binding of the transcription factor to its target elements (17–19). A different mechanism is for the antiactivator to occlude sequences required for requisite multimerization of transcription factors into their active form (20, 21). The TraR–TraM complex structure we report here provides a different mechanism by which the antiactivator allosterically prevents DNA binding by indirectly altering the conformation of the DNA binding domain, preventing productive interactions with DNA-binding sites. This allosteric mechanism of inhibition may be more broadly used by antiactivators than is currently appreciated for transcription regulation and complex signal transduction pathways.

Materials and Methods

Protein Expression and Purification. The *traM* and *traR* genes from *Rhizobium* sp. strain NGR234 were cloned into pET11a (Novagen, Madison, WI) and pET23b (Novagen) overexpression vectors, and the plasmids were transformed into *Escherichia coli* BL21(DE3)

codon plus and Rosetta 2, respectively. To overexpress TraM$_{NGR}$, cells were grown in LB to an OD$_{600}$ of 0.8 at 37°C and induced for 5 h with isopropyl-β-D-thiogalactopyranoside (0.4 mM). To overexpress TraR$_{NGR}$, after cells were grown in LB at 37°C to an OD$_{600}$ of 0.6, *N*-(3-oxo-octanoyl)-L-homoserine lactone (25 μM) and isopropyl-β-D-thiogalactopyranoside (0.1 mM) were added, and the culture was grown 5 h at 25°C.

To purify TraM$_{NGR}$, cells were lysed in 50 mM sodium phosphate (pH 8.0)/0.5 mM EDTA/1 mM DTT/50 mM NaCl by using a continuous flow microfluidizer (MicroFluidics, Taylorsville, UT). Clear cell lysate was loaded on a FastQ column (Amersham Biosciences, Piscataway, NJ) and eluted with a gradient of NaCl (0.05–1 M). Fractions containing TraM$_{NGR}$ were concentrated, exchanged to 50 mM Tris·Cl (pH 8.0)/200 mM NaCl/0.5 mM EDTA/1 mM DTT and purified by using a Superdex75 column (Amersham Biosciences). For TraR$_{NGR}$ purification, cells were lysed in 50 mM imidazole (pH 8.0)/0.5 mM EDTA/300 mM NaCl/1 mM DTT/5% glycerol. Cell-free lysate was loaded onto a Heparin column (Amersham Biosciences) and eluted with a NaCl gradient (0.30–1 M). Fractions containing TraR$_{NGR}$ were concentrated, exchanged to 50 mM imidazole (pH 8.0)/300 mM NaCl/0.5 mM EDTA/1 mM DTT, and size fractionated on a Superdex75 column. To prepare the TraM$_{NGR}$–TraR$_{NGR}$ complex, purified TraR$_{NGR}$ and TraM$_{NGR}$ were mixed at a molar ratio of 1:2 and incubated at 4°C overnight in 50 mM imidazole (pH 8.0)/1 M NaCl/0.5 mM EDTA/1 mM DTT. The solution was concentrated and size fractionated on a Superdex200 column (Amersham Biosciences).

AUC Experiments. Sedimentation equilibrium experiments were carried out by using an XL-A analytical ultracentrifuge (Beckman, Fullerton, CA). Protein samples were dialyzed extensively against a buffer containing 50 mM Hepes (pH 8.0), 300 mM NaCl, 1 mM β-methylphenylalanine, 0.5 mM EDTA, and 5% glycerol. For each protein, absorbances at 280, 275, and 285 nm were measured for three protein concentrations (0.15 mg/ml, 0.3 mg/ml, and 0.5 mg/ml) and different rotor speeds (TraM$_{NGR}$, 35,000 rpm; TraR$_{NGR}$, 26,000 rpm; TraM$_{NGR}$–TraR$_{NGR}$, 20,000 rpm) at 4°C. Sedimentation equilibrium profiles were analyzed by using the Windows (Microsoft, Redmond, WA) version of Ultrascan 8.0 (University of Texas Health Science Center, San Antonio, TX).

ITC Experiments. ITC experiments were carried out at 25°C in a VP-ITC titration calorimeter system (MicroCal, Northampton, MA). Purified TraR$_{NGR}$ (120 μM) and TraM$_{NGR}$ (11.4 μM) were dialyzed in 50 mM imidazole (pH 7.0), 300 mM NaCl, 0.5 mM EDTA, and 1 mM β-mercaptoethanol. Thirty aliquots of 10-μl samples of TraR$_{NGR}$ were injected into the TraM$_{NGR}$ solution at 240-s intervals. Data were processed with the Origin software (OriginLab, Northampton, MA), and thermodynamic parameters of the binding process were derived by fitting the corrected binding isotherm to a single-site binding model.

Crystallization and Data Collection. The TraM$_{NGR}$–TraR$_{NGR}$ complex was crystallized by hanging-drop vapor diffusion by mixing an equal volume of the complex [8 mg/ml in 50 mM imidazole (pH 7.0)/300 mM NaCl/0.5 mM EDTA/1 mM DTT] with the well solution [1 mM DTT with 60 mM Hepes (pH 7.5),/120 mM CaCl$_2$/16.8% PEG400]. Crystals were flash frozen in the well solution with a 10% increment of every ingredient plus 17% polyethylene glycol and 15% glycerol. Data were collected at ALS Beamline 4.2.2 (Advanced Light Source, Berkeley, CA) and processed by using d*trek software (22). The crystal belonged to the P1 space group (a = 56.91 Å, b = 62.50 Å, c = 65.50 Å, α = 94.89°, β = 110.47°, and γ = 99.18°) with one heterotetramer TraR$_{NGR}$–TraM$_{NGR}$ complex per asymmetric unit.

Structure Determination. The structure was solved by molecular replacement by using Phaser (23). Briefly, the two NTDs of TraR$_{NGR}$ were located by using the NTD of TraR$_{At}$ (Protein Data Bank ID code 1L3L) as the initial model, and after refinement of the partial model by using Crystallography & NMR System software (24), one CTD was subsequently identified. The second CTD was found after refinement and rebuilding of the more complete model. Further refinement and noncrystallographic symmetry averaging with the use of MAMA (25) gave rise to electron density for two TraM$_{NGR}$ molecules, the model for which was subsequently built by using ARP/wARP (26). Further model building was performed manually in O (27), and the model was refined by using Crystallography & NMR System software (24). Crystallographic statistics are summarized in SI Table 1.

1. Waters CM, Bassler BL (2005) *Annu Rev Cell Dev Biol* 21:319–346.
2. Fuqua C, Greenberg EP (2002) *Nature Rev* 3:685–695.
3. Zhang LH, Dong YH (2004) *Mol Microbiol* 53:1563–1571.
4. Wang C, Zhang HB, Chen G, Chen L, Zhang LH (2006) *J Bacteriol* 188:2435–2445.
5. Fuqua C, Burbea M, Winans SC (1995) *J Bacteriol* 177:1367–1373.
6. Hwang I, Cook DM, Farrand SK (1995) *J Bacteriol* 177:449–458.
7. He X, Chang W, Pierce DL, Seib LO, Wagner J, Fuqua C (2003) *J Bacteriol* 185:809–822.
8. Swiderska A, Berndtson AK, Cha MR, Li L, Beaudoin GM, III, Zhu J, Fuqua C (2001) *J Biol Chem* 276:49449–49458.
9. Luo ZQ, Qin Y, Farrand SK (2000) *J Biol Chem* 275:7713–7722.
10. Chen G, Malenkos JW, Cha MR, Fuqua C, Chen L (2004) *Mol Microbiol* 52:1641–1651.
11. Chen G, Wang C, Fuqua C, Zhang LH, Chen L (2006) *J Bacteriol* 188:8244–8251.
12. Vannini A, Volpari C, Di Marco S (2004) *J Biol Chem* 279:24291–24296.
13. Qin Y, Su S, Farrand SK (2007) *J Biol Chem* 282:19979–19991.
14. Luo ZQ, Smyth AJ, Gao P, Qin Y, Farrand SK (2003) *J Biol Chem* 278:13173–13182.
15. Vannini A, Volpari C, Gargioli C, Muraglia E, Cortese R, De Francesco R, Neddermann P, Marco SD (2002) *EMBO J* 21:4393–4401.
16. Zhang RG, Pappas T, Brace JL, Miller PC, Oulmassov T, Molyneaux JM, Anderson JC, Bashkin JK, Winans SC, Joachimiak A (2002) *Nature* 417:971–974.
17. Navarro-Aviles G, Jimenez MA, Perez-Marin MC, Gonzalez C, Rico M, Murillo FJ, Elias-Arnanz M, Padmanabhan S (2007) *Mol Microbiol* 63:980–994.
18. Mol CD, Arvai AS, Sanderson RJ, Slupphaug G, Kavli B, Krokan HE, Mosbaugh DW, Tainer JA (1995) *Cell* 82:701–708.
19. Liu D, Ishima R, Tong KI, Bagby S, Kokubo T, Muhandiram DR, Kay LE, Nakatani Y, Ikura M (1998) *Cell* 94:573–583.
20. Chai Y, Zhu J, Winans SC (2001) *Mol Microbiol* 40:414–421.
21. Masuda S, Bauer CE (2002) *Cell* 110:613–623.
22. Pflugrath JW (1999) *Acta Crystallogr D Biol Crystallogr* 55:1718–1725.
23. McCoy AJ, Grosse-Kunstleve RW, Storoni LC, Read RJ (2005) *Acta Crystallogr D Biol Crystallogr* 61:458–464.
24. Brunger AT, Adams PD, Clore GM, DeLano WL, Gros P, Grosse-Kunstleve RW, Jiang JS, Kuszewski J, Nilges M, Pannu NS, *et al.* (1998) *Acta Crystallogr D Biol Crystallogr* 54:905–921.
25. Kleywegt GJ (1994–2007) MAMA (Uppsala Software Factory, Uppsala) Version 070626.
26. Morris RJ, Perrakis A, Lamzin VS (2003) *Methods Enzymol* 374:229–244.
27. Jones TA, Zou JY, Cowan SW, Kjeldgaard M (1991) *Acta Crystallogr A* 47:110–119.
28. Kraulis P (1991) *J Appl Crystallogr* 24:946–950.
29. Merritt EA, Bacon DJ (1997) *Methods Enzymol* 277:505–524.
30. Chenna R, Sugawara H, Koike T, Lopez R, Gibson TJ, Higgins DG, Thompson JD (2003) *Nucleic Acids Res* 31:3497–3500.

BIOCHEMISTRY